Pramāṇa, Vol. 15, No. 3, September 1980, pp. 309–326. © Printed in India.

Momenta and rapidity characteristics of the multiparticle production in 50 GeV/c π^--Emulsion collison

V KUMAR, N S VERMA, S C VARMA and A P SHARMA
Department of Physics, Kurukshetra University, Kurukshetra 132 119, India

MS received 13 July 1979; revised 11 August 1980

Abstract. The momenta and rapidity characteristics of the particles produced in 50 GeV/c π^--collision with emulsion nuclei have been studied with an emulsion stack exposed under a pulsed magnetic field. The longitudinal rapidity plots suggest that leading pion is attenuated strongly when passing through a heavy nucleus. The average net charge $\langle N_s^+ - N_s^- \rangle$ produced in the final state of the reaction rises rapidly from a negative to a positive value at $N_h \leqslant 1$ and attains a constant value $\simeq 0{\cdot}60 \pm 0.08$ at all $N_h \geqslant 7$.

Keywords. Multiparticles; proton emission; rapidity; attenuation of the leading pion; parton-model; rescattering effect.

1. Introduction

Since the parton-picture of high energy hadron has been hypothesised by Feynman (1969), multiparticle production in hadron-hadron, hadron-nucleus, lepton-lepton and lepton-nucleus collisions have been extensively studied. The lepton-hadron and hadron-hadron reactions are useful to establish the parton hypothesis while the hadron nucleus and lepton-nucleus reactions help to study the space-time development of hadronic matter. The energy flux cascade model (Gottfried 1973) is one of the initial steps in this direction. In fact, the space-time picture of the hadronic matter is related to the scattering mode of the projectile with the nuclear matter and its energy characteristics after the collision takes place. Due to insufficient experimental data on the leading-particle-effect in hadron-nucleus collision Gottfried (1973) assumed the effect to be the same as in hadron-nucleon* collision, although this does not seem to be true.

The present experiment was designed to study the energy-momenta characteristics of the multiparticles produced in the final state of 50 GeV/c π^--collision with emulsion nuclei. For this purpose an NIKFI-R emulsion stack exposed to a narrow-beam of negative pions in the pulsed magnetic field of strength $\simeq$ 180 KGauss has been used.

*In hadron-nucleon collision the leading particle appears in the final state of the reaction with nearly 50% of the initial momentum and containing internal quantum numbers of the projectile hadron.

2. Experimental details

201 interactions of 50 GeV/c π^--mesons with all emulsion nuclei lying in the middle layers of the emulsion pellicle (i.e. 50 to 220 μm from the air side) were taken up (Kumar *et al* 1978). The momentum of shower particles ($\beta > 0{\cdot}7$) produced in the reaction was measured by the magnetic curvature technique (Tolstov and Shabratova 1974). Using the three-point deflection method (Denysz *et al* 1963). Y-coordinates on the particle trajectory at three equally spaced (X=0, X=t and X=2t=L (cm)) points were noted. The second difference, D_{mag} is proportional to the angle of deflection/curvature of the track. D_{mag} is related to the particle momentum with the following relation,

$$P_{\text{lab (GeV/c)}} = \frac{3\times 10^{-4}\, Ht^2}{\mid D \mid_{\text{mag}} \cos\delta} \tag{1}$$

where H is the strength of magnetic field in KGauss and δ the angle of dip of the particle track. In measuring D_{mag} the main contribution to the noise arises from the multiple coulomb scattering and distortions. Errors in D_{mag} and uncertainty in the magnetic pulse contribute to errors in momentum measurement. The P_{lab} errors may be expressed as

$$(\Delta P/P)^2 = (\Delta H/H)^2 + (\Delta D/D)^2, \tag{2}$$

where
$$(\Delta D/D)^2 = (\Delta D/D)^2_{\text{coul.}} + (\Delta D/D)^2_{\text{dis.}}. \tag{3}$$

However, as pointed out by Tolstov and Shabratova (1974) distortions may not be considered as a first order approximation in very strong fields $\simeq 10^6$ Gauss for particle measurement with momentum $\leqslant$ 50 GeV/c. To minimise distortion effects and choose tracks for measurement we use the following criteria and assumptions:

(i) The interactions lying within 50 μm from the air side and 50 μm from the bottom side layers of emulsion are not considered. (ii) The track segment lying in nearly 25 μm from the air and 25 μm from the glass surface layers are not measured. Also, the track segments and the interactions within a 'cut-off' region of nearly 5 mm all around the pellicle-edge are discarded. The emulsion pellicles are circular with diameter approximately 6·2 cm and their thickness before development was $\sim$ 610 μm (iii) The tracks with available projected length less than 500 μm and (iv) the tracks which suffer more than one nuclear-scattering at consecutive points less than 400 μm apart are not considered. The total number of such tracks is 89 out of a total of 1730 shower tracks belonging to 201 interactions. Besides, the maximum possible length of the track available in the pellicle of its origin has been followed.

Table 1 details the measured tracks i.e. percentage of measured and unmeasured tracks and relative error $\Delta P/P_{\text{lab}}$ in different θ_{lab}-bins. These details are also displayed in figures 1(a), (b) and (c). Figure 1(a) displays the measured length distribution of 1641 tracks in θ_{lab}-bins while in figure 1(b) the percentage of measured and unmeasured tracks in different θ_{lab}-bins along with the average projected

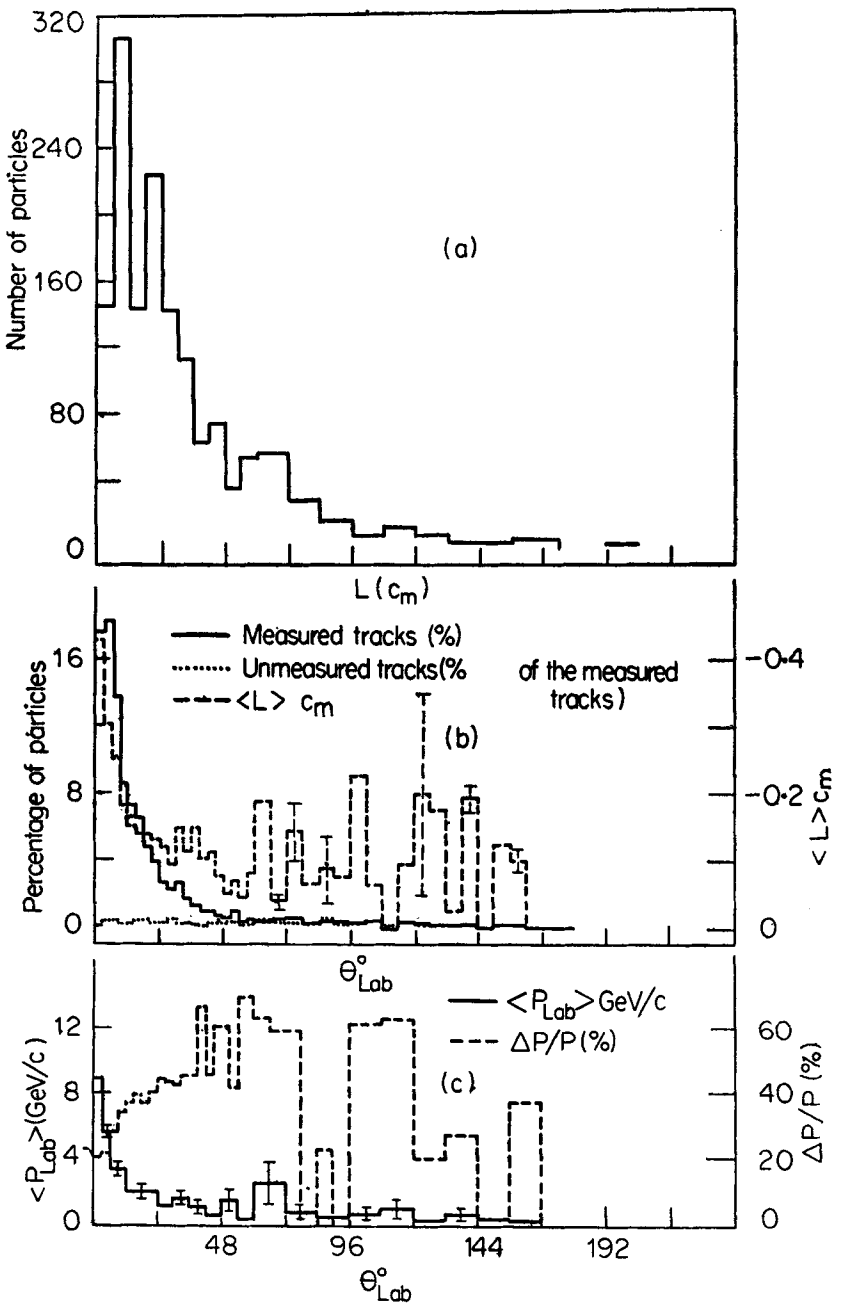

Figure 1. (a) Measured track length plot. (b) (i) Percentage of particle tracks (ii) Percentage of unmeasured tracks with respect to measured tracks. (iii) Average track length. (c) Average momentum and relative percentage error versus θ°_{lab} plots.

track length, $\langle L \rangle$ (cm) are given. In figure 1(c) the average momentum P_{lab} and the relative error ($\Delta P/P\%$) in different θ_{lab}-bins are given. It is seen that the percentage of measured tracks and their average measured length are larger at smaller angles. Similarly, P_{lab} is larger at smaller angles while $\Delta P/P$ is smaller at small angles.

Table 1. Angular details of the average track length, $\langle L \rangle$ cm and the errors in momentum P_{lab} of the particle

θ_s -interval	Measured tracks (%)	Unmeasured tracks (%)	Average track length	Error in P_{lab}
0 -3°	17.77	0·139	0.428	19.00
3 -6°	18·25	0·348	0·301	21·60
6 -12°	22.09	0·557	0·221	30.45
12-24°	22.44	1·045	0.140	38·10
24-36°	09·34	1.185	0.119	43·62
36-60°	06·27	1·394	0·098	55·51
60-90°	02·02	1.672	0.104	63.07
>90°	01.81	0.906	0.121	43·55

This is because the major contributing factor to the errors is the multiple coulomb scattering which has a relation with the magnetic deflection,

$$D_{coul}/D_{mag} = (\Delta D/D_{coul}) = K/(1{\cdot}72 H_{eff}\, t^{1/2}) \tag{4}$$

where K is the scattering constant, $t=L/2$ is the cell length and H_{eff} is the effective strength of the pulsed magnetic field which is mainly a function of the cell length used in the measurements. H_{eff} is evaluated by measuring D_{mag} on the primary tracks of known momentum (50 GeV/c). Thus putting the value of D_{mag} and $P=50$ GeV/c in relation (1) one can find out H_{eff}. Figure 2 shows a histogram of H_{eff} for 150 primary tracks lying in the middle layers of the emulsion pellicles. These measurements were made in a separate study by Kumar (1979). The average value $\langle H_{eff} \rangle$ comes out to be 167·50 $\pm$ 3·54 KGauss.

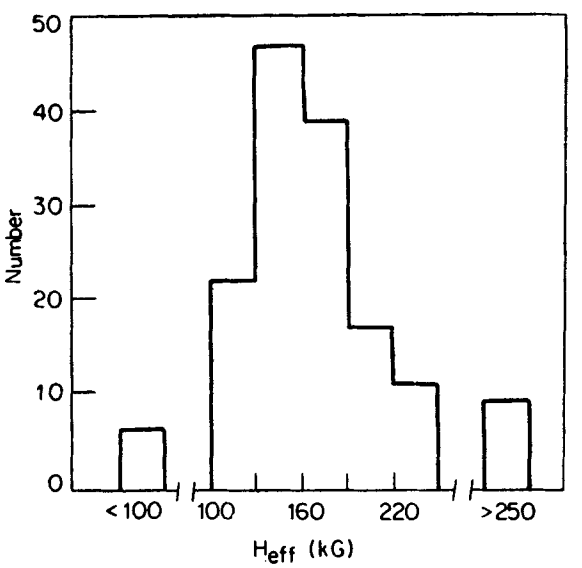

Figure 2. H_{eff} plot.

To assign charge polarity to the shower particles it has been assumed that they are all singly-charged. Considering that the primary particle is negatively charged, the shower particles are assigned polarity by comparing the directions of the centre of curvature of the shower track with respect to the primary particle track.

3. Experimental results and discussion

3.1 *General characteristics of shower particles*

In figure 3, the momentum P_{lab} of shower particles of both negative and positive polarity has been shown separately in the three bins i.e. (a) $P_{lab} \leqslant 3{\cdot}5$ GeV/c (b) $3{\cdot}5 < P_{lab} \leqslant 10$ GeV/c and (c) $P_{lab} > 10$ GeV/c. In table 2 the average multiplicity of N_s^- and N_s^+ particles separately has been shown in different P_{lab} and N_h-bins ($N_h = N_b + N_g$, are the particles with $\beta < 0{\cdot}7$). In the momentum interval $P_{lab} \leqslant 3{\cdot}5$ GeV/c, the N_s^+ particles dominate N_s^- particles up to say 1 GeV/c and in $3{\cdot}5 < P_{lab} \leqslant 10$ GeV/c interval, the two distributions are almost the same. In the momentum bin > 10 GeV/c or $P/P_0 > 0{\cdot}2$ N_s^- dominates over N_s^+ particles. These agree with the results of Vionov *et al* (1975, 1977).

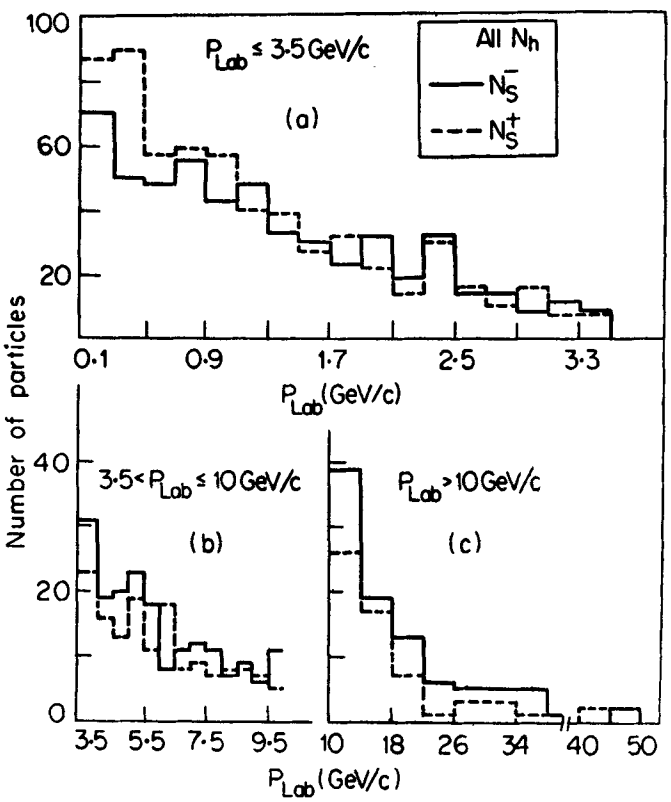

Figure 3. P_{lab} distributions for N_s^- and N_s^+ **separately.**

Table 2. Average number of shower particles in different P_{lab}-bins (P_0=50 GeV/c, projectile momentum)

P/P_0	Average multcipliities					
	$N_h \leqslant 1$		$N_h \leqslant 6$		$N_h \geq 7$	
	N_s^+	N_s^-	N_s^+	N_s^-	N_s^+	N_s^-
>0·5	1·52 ± 0·27	2·42 ± 0·43	1·44 ± 0·14	1·73 ± 0·17	1·22 ± 0·13	1·62 ± 0·12
>0·10	0·87 ± 0·16	1·58 ± 0·28	0·95 ± 0·09	1·10 ± 0·11	0·62 ± 0·06	1·01 ± 0·11
>0·20	0·29 ± 0·05	0·58 ± 0·10	0·35 ± 0·03	0·51 ± 0·05	0·23 ± 0·02	0·45 ± 0·05
>0·40	0·06 ± 0·01	0·10 ± 0·02	0·08 ± 0·01	0·14 ± 0·01	0·05 ± 0·005	·14 ± 0·01

Table 3. Some characteristics of P_{lab} -distributions of fast secondaries in 50 GeV/c π^--e.m. collision

Characteristic	$P_{lab} \leqslant 3{\cdot}5$	$3{\cdot}5 < P_{lab} \leqslant 10$	$P_{lab} > 10$
N_s^-/N_s^+ ratio	0·88	1·22	1·58
$\langle P_{lab} \rangle$ for N_s^-	1·278 ± 0·037	5·978 ± 0·136	18·842 ± 0·878
$\langle P_{lab} \rangle$ for N_s^+	1·157 ± 0·034	6·016 ± 0·144	17·483 ± 0·981

In table 3, the negative-to-positive particle ratio N_s^-/N_s^+ and $\langle P_{lab} \rangle$ in different P_{lab} bins has been given. It can be seen that this ratio increases with increase of momentum and $\langle P_{lab} \rangle$ is almost the same in all bins for both N_s^- and N_s^+ particles.

In figure 4, the differential distribution of longitudinal momentum P_L has been plotted for N_s^- and N_s^+ particles separately. The suffix i in the y-coordinate corresponds to the polarity of the secondary particles. It may be observed that at all $P_L < 1{\cdot}0$ GeV/c the N_s^+ particles dominate N_s^- presumably due to the recoiling target protons amongst showers.

In figure 5, the average net charge $\langle N_s^+ - N_s^- \rangle$ has been plotted with respect to N_h to study the fragmentation effect of the heavy nuclei. It is seen that $\langle N_s^+ - N_s^- \rangle \simeq 0{\cdot}60 \pm 0{\cdot}08$ at all $N_h \geqslant 7$. The events with $N_h \geqslant 7$ may be contributed largely by the AgBr nuclei of the emulsion composition. Vionov *et al* (1977) obtained a net charge of $0{\cdot}70 \pm 0{\cdot}10$ for $N_h \geqslant 7$ which agrees with our results and necessarily points out the suppression of the excess negative charge of leading particles at higher N_h values. The dominance of positive charge at higher N_h (or equivalently larger target mass) may however be due to the recoiling protons.

In figure 6, different distributions of transverse momentum, P_T for N^- and N_s^+ particles have been plotted for (a) $N_h \leqslant 1$ (b) $\leqslant 7$ and (c) $\geqslant 8$ groups of events. The following observations can be made: (i) N_s^- and N_s^+ particle distributions seem to be similar in the first and second bins while in the third the N_s^+ particles dominate the N_s^- particle distribution at $P_T \leqslant 0{\cdot}5$ GeV/c. (ii) In all the three N_h-bins the P_T range extends almost equally to large P_T (i.e. $> 2{\cdot}0$ GeV/c) in both N_s^- and N_s^+ particles. The large number of particles is limited to small P_T.

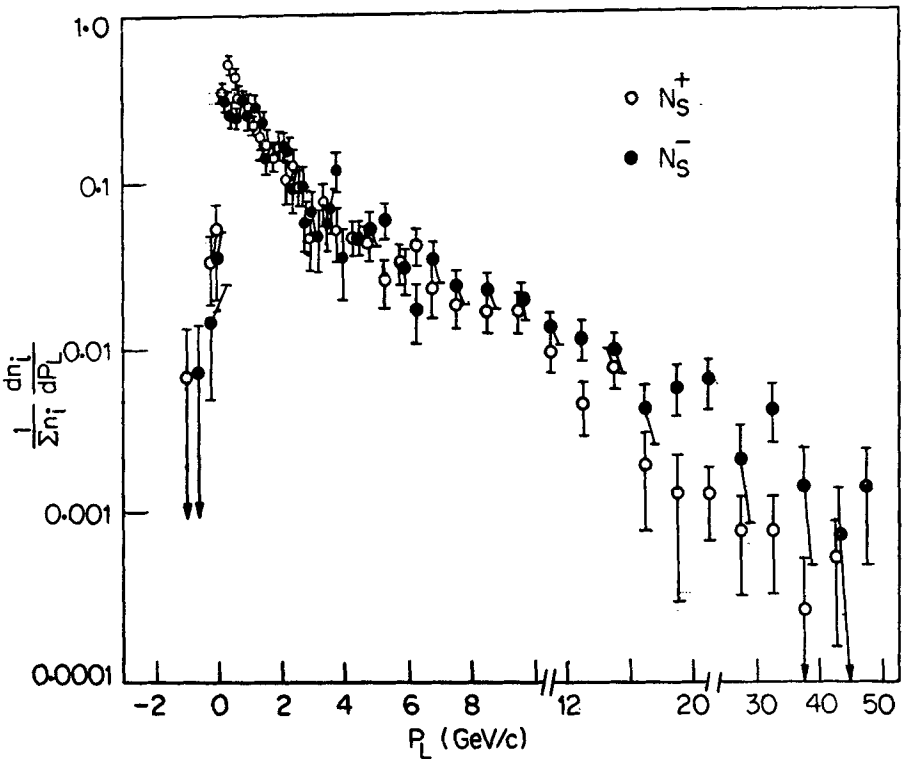

Figure 4. Differential distribution of N_s^- and N_s^+ particles separately plotted with respect to longitudinal momentum.

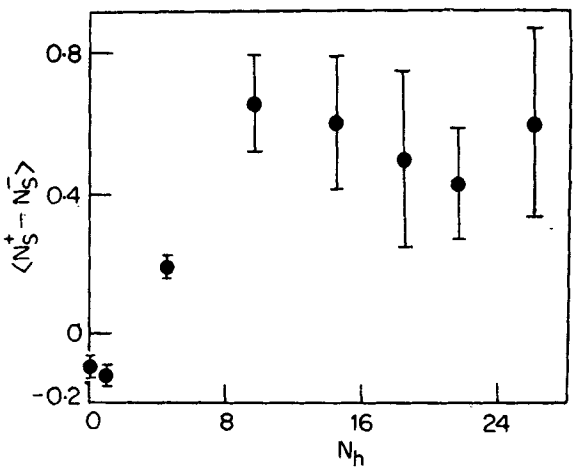

Figure 5. Average net charge plotted with respect to N_h.

In table 4, $\langle P_T \rangle$ for N_s^- and N_s^+ particles separately has been given in $\leqslant 2{\cdot}0$ and $> 2{\cdot}0$ bins for $N_h \leqslant 1$, $N_h \leqslant 7$ and $N_h \geqslant 8$ events. It may be noted that $\langle P_T \rangle$ of N_s^- particles is higher than that of N_s^+ in almost all N_h-bins.

In figure 7 the invariant cross-section

$$\frac{Ed\sigma^3}{dP^3} \equiv \frac{1}{\pi}\frac{d\sigma^2}{dy\, dP_T^2}$$

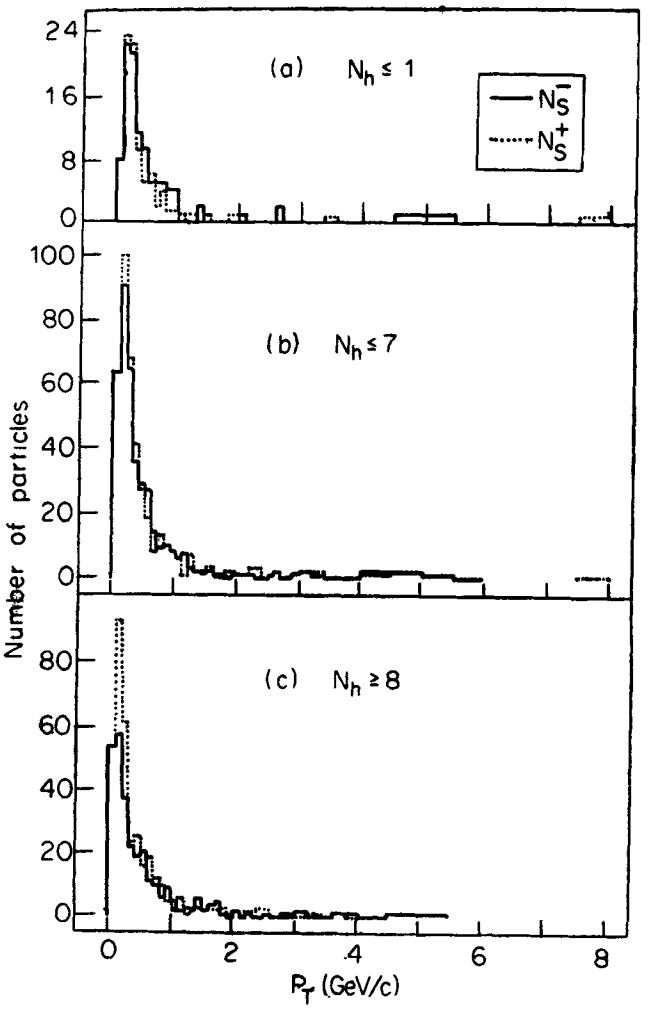

Figure 6. Differential distributions of transverse momentum for N_s^- and N_s^+ particles.

has been plotted with respect to P_T for N_s^- and N_s^+ particles respectively. In both cases, the distributions in $P_T \leqslant 0{\cdot}6$ GeV/c region are well explained by exp $(-P_T/m_\pi)$ curve (giving a χ^2 per data point=18·66/6 and 17·72/6 for N_s^- and N_s^+ distributions respectively). The exponential fall of the cross-section favours the hydrodynamical model which in principle adopts the statistical behaviour of the hadronic matter. In the large $-P_T$ region the $Ed\sigma^3/dP^3 \propto P_T^{-4}$ power law has been fitted to the data which gives χ^2 per data point=5·086/6 for N_s^- particles and 11·47/7 for N_s^+ particles. It may, however, be mentioned that the statistics of the large P_T data is quite small. The P_T^{-4} power law supports the parton-model of Berman *et al* (1971), popularly known as the BBK-model which considers the hard scattering of the constituent quarks of hadrons by the exchange of a vector-gluon. The process is scale-invariant. The modified quark model due to Gunion *et al* (1972) however suggests the P_T^{-8} power law in the elementary reactions. Thus P_T^{-4} law giving much

Table 4. $\langle P_T \rangle$ of N_s^- and N_s^+ particles in different N_h bins

P_T (GeV/c)	$N_h \leqslant 1$		$N_h < 7$		$N_h \geqslant 8$		All N_h	
	N_s^-	N_s^+	N_s^-	N_s^+	N_s^-	N_s^+	N_s^-	N_s^+
< 2·0	0·404 ± 0·032	0·343 ± 0·078	0·360 ± 0·017	0·354 ± 0·026	0·438 ± 0·026	0·373 ± 0·020	0·395 ± 0·015	0·363 ± 0·013
All P_T	0·551 ± 0·076	0·453 ± 0·091	0·475 ± 0·035	0·432 ± 0·032	0·537 ± 0·042	0·445 ± 0·033	0·503 ± 0·031	0·438 ± 0·022

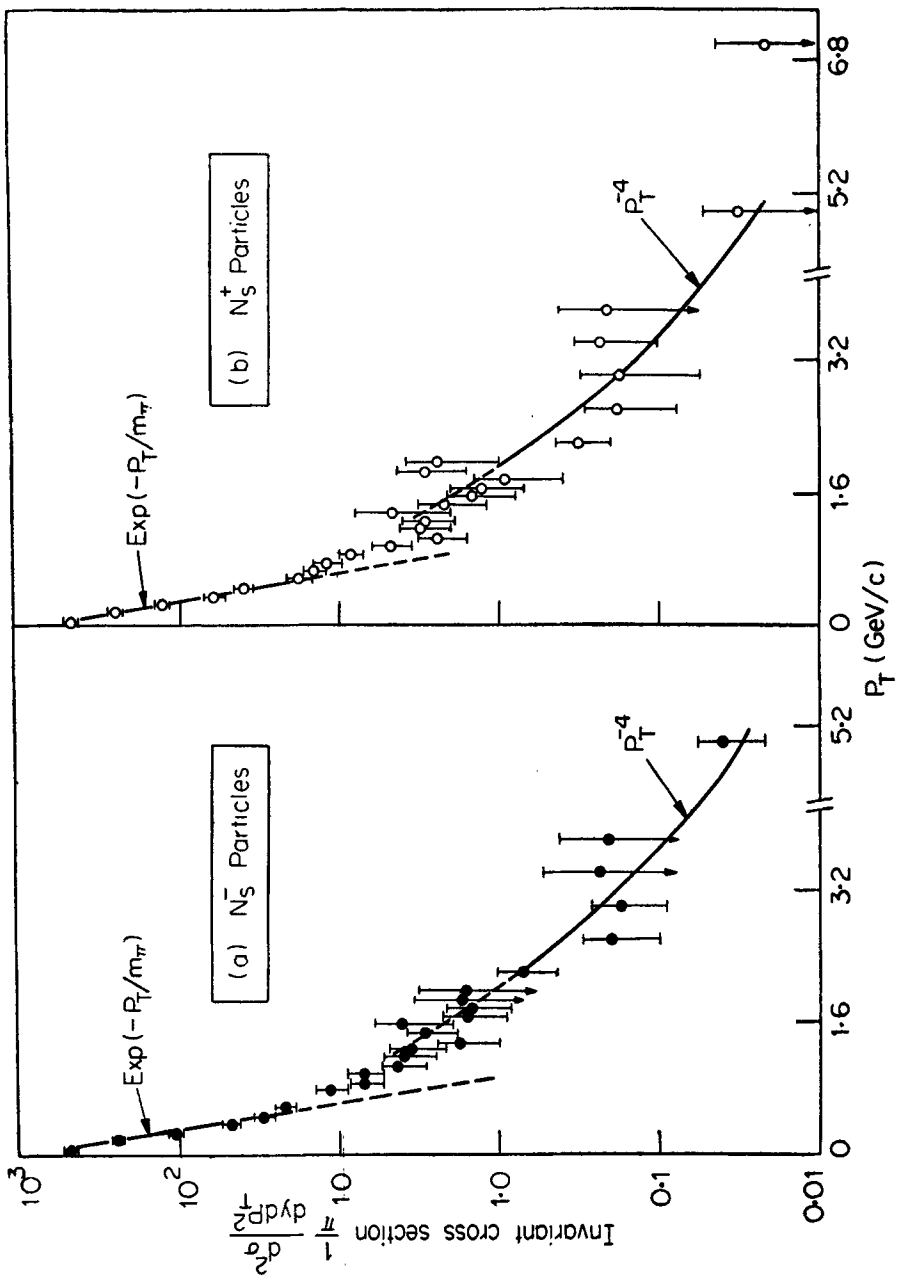

Figure 7. Plots of invariant cross-section with respect to P_T in GeV/c π^--Em collision.

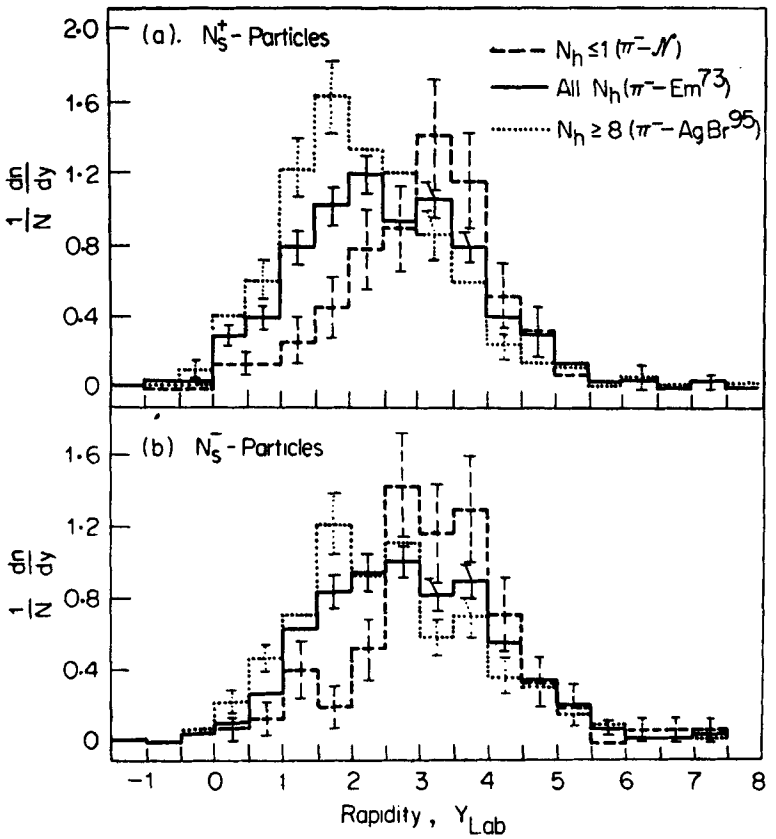

Figure 8. Differential plots of longitudinal rapidity.

higher value than P_T^{-8} law suggests the possibility of rescattering effect. In figures 7(a) and (b) if the P_T^{-4} curve is extrapolated in smaller P_T region, one finds that it explains the data upto $P_T \simeq 1{\cdot}0$ GeV/c.

In figures 8(a) and (b) the differential distributions in longitudinal rapidity Y_{lab}, defined by Feynman (1969) and given by the expression,

$$Y_{\text{lab}} = -\ln \frac{(E - P_L)}{(P_T^2 + m^2)^{1/2}}, \tag{5}$$

have been plotted for N_s^+ and N_s^- particles respectively. The distributions are plotted for (i) $N_h \leqslant 1$, (ii) all N_h and (iii) $N_h \geqslant 8$ bins to study the target mass dependence of rapidity. It is observed that (i) in the $Y_{\text{lab}} \leqslant 2{\cdot}0$ region the distribution corresponding to higher N_h bin dominates to lower N_h. This region is called the target fragmentation region and (ii) the behaviour of both N_s^- and N_s^+ particles is not distinguishable in the central rapidity i.e. $2{\cdot}0 < Y_{\text{lab}} \leqslant 4{\cdot}0$ in the high rapidity $Y_{\text{lab}} > 4{\cdot}0$ region as well.

To study the transverse momentum dependence on the longitudinal momentum, we plot the differential P_T distribution in rapidity intervals (*a*) $Y_{\text{lab}} > 3{\cdot}5$, (b) $1{\cdot}5 < Y_{\text{lab}} \leqslant 3{\cdot}5$ and (c) $Y_{\text{lab}} \leqslant 1{\cdot}5$ for both N_s^- and N_s^+ particles separately in figure 9. It is clear that both distributions are limited to $P_T < 2{\cdot}0$ GeV/c and are

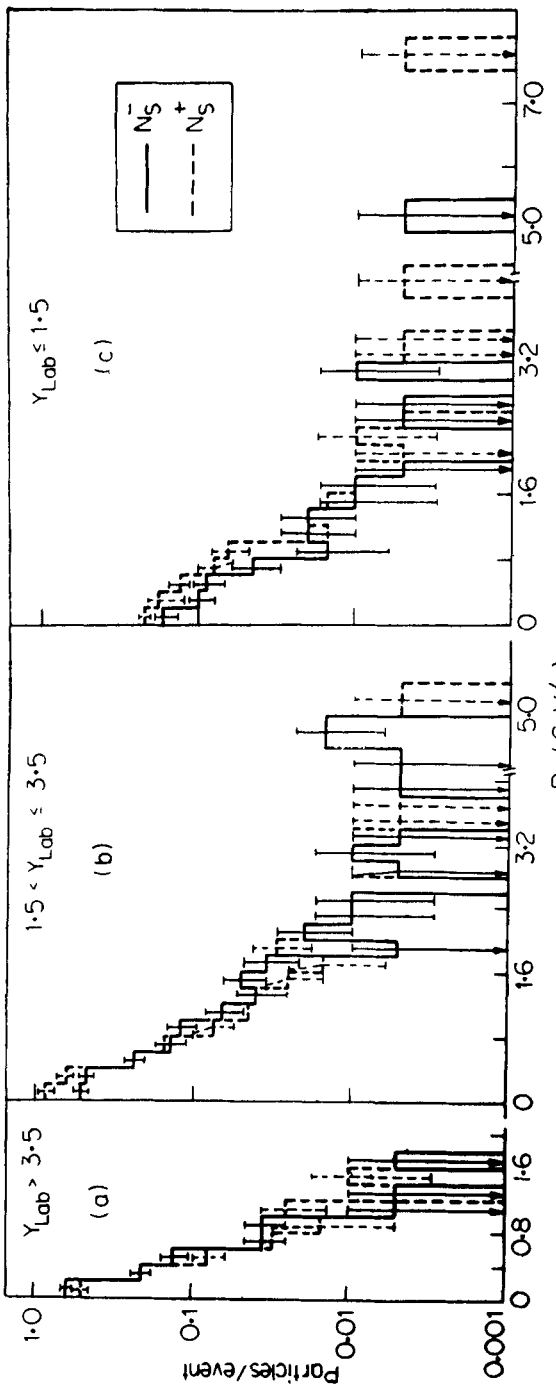

Figure 9. Average multiplicity of N_s^+ and N_s^- particles plotted with respect to P_T.

Table 5. $\langle P_T \rangle$ of N_s^- and N_s^+ particles in different Y_{lab} and P_T intervals.

P_T — interval (GeV/c)	$Y_{lab} > 3{\cdot}5$		$1{\cdot}5 < Y_{lab} \leqslant 3{\cdot}5$		$Y_{lab} \leqslant 1{\cdot}5$	
	N_s^-	N_s^+	N_s^-	N_s^+	N_s^-	N_s^+
0 — 0·6	0·199 ± 0·014	0·193 ± 0·015	0·255 ± 0·016	0·227 ± 0·012	0·254 ± 0·029	0·268 ± 0·026
0 — 1·0	0·239 ± 0·014	0·223 ± 0·014	0·398 ± 0·014	0·289 ± 0·011	0·323 ± 0·025	0·379 ± 0·022
0 — 2·0	0·255 ± 0·017	0·263 ± 0·020	0·465 ± 0·024	0·355 ± 0·018	0·462 ± 0·043	0·423 ± 0·033
> 2·0	—	—	3·106 ± 0·237	2·933 ± 0·232	3·330 ± 0·980	3·500 ± 0·619
All P_T	0·255 ± 0·017	0·263 ± 0·020	0·590 ± 0·038	0·437 ± 0·028	0·599 ± 0·076	0·579 ± 0·069

the same for N_s^- and N_s^+ particles. There is absolutely no particle with $P_T \geqslant 2{\cdot}0$ GeV/c produced due to a hard scattering or violent collision (Meng Ta Chung, 1977). In figure 9(b) both the distributions are extended to large P_T except that N_s^+ particles exceed N_s^- in $P_T < 0{\cdot}4$ GeV/c region. The distributions in figure 9(c) suggest that at $P_T < 1{\cdot}0$ GeV/c N_s^+ distributions are extended to large P_T region. Table 5 displays the numerical results of $\langle P_T \rangle$ in the three rapidity regions for different P_T-intervals. The following observations may be made: (i) $\langle P_T \rangle$ of N_s^- and N_s^+ particles are almost the same in $Y_{\text{lab}} > 3{\cdot}5$ region and all P_T intervals. (ii) $\langle P_T \rangle$ of N_s^- is larger than that of N_s^+ particles in the central Y_{lab} region in all P_T intervals, which in turn suggests a rescattering effect. (iii) In the $Y_{\text{lab}} \leqslant 1{\cdot}5$ region $\langle P_T \rangle$ of N_s^+ particles is larger than that of N_s^- particles in $P_T < 0{\cdot}6$ GeV/c and $P_T < 1{\cdot}0$ GeV/c intervals. At higher P_T, the two data are almost comparable. The production of N_s^+ particles with large — P_T at small rapidities suggests the production of fragments (or more likely the protons) with relatively smaller momentum but at large angles.

3.2 *Attenuation of leading pion*

In an angular study of shower particles in 50 GeV/c π^--Em collision by Kumar *et al* (1978), it has been shown that at high pseudo-rapidity the leading particle multiplicity is very much smaller than unity in the events with heavy nuclei as compared to the π^--nucleon interaction. The effect may be called the attenuation of leading particle. Here we investigate the effect with the help of the momenta and the rapidity characteristics of the shower particles. We assume that the events with $N_h \leqslant 1$ are similar to π^--nucleon interactions. The $\langle N_s \rangle$ value in $N_h = 0$ and $N_h = 1$ bins is almost equal and its magnitude being equal to $5{\cdot}77 \pm 0{\cdot}32$ and $5{\cdot}54 \pm 0{\cdot}32$ respectively while $\langle N \rangle_{\text{ch}H}$ for 50 GeV/c π^--p collision from the bubble chamber experiment has been given to be $5{\cdot}71 \pm 0{\cdot}13$ by Ammosov *et al* (1973).

In figures 10(a), (b) and (c) the normalised multiplicity $R_A = [(n_s)_A / (N_s)_H]_{Y_{\text{lab}}}$ plots have been made with respect to rapidity, Y_{lab} for the combined $N_s^{\pm}$ multiplicity; for separate N_s^- and N_s^+ multiplicities in π^--Em reaction and for π^--AgBr reaction respectively. For π^--AgBr reaction the data of $N_h \geqslant 8$ have been used. In defining R_A, the multiplicity data of $N_h \leqslant 1$ events have been used for π^--nucleon interactions.

From figures 10 (a) and (b) it is clear that (i) $R_{\text{em}}\ (Y) > 1$ and its averaged value $\simeq 2{\cdot}3 \simeq \langle \nu_{\text{em}} \rangle$ in the target region ($Y_{\text{lab}} \leqslant 2{\cdot}0$). $\langle \nu_{\text{em}} \rangle$ is the average number of encounters of the projectile in passing through the emulsion nuclei. (ii) In the interval $2{\cdot}5 < Y_{\text{lab}} < 4{\cdot}5$, $R_{\text{em}} \simeq 0{\cdot}68 \pm 0{\cdot}18$ and there appears a dip probably caused due to the absorption of some of the produced particles inside the target nucleus itself. This may cause, in turn, intra-nuclear cascading, as a result of which $R_{\text{em}} > 1$ in the target region. (iii) In the rapidity interval $4{\cdot}75 < Y_{\text{lab}} \leqslant 6{\cdot}0$, $R_{\text{em}} \geqslant 1$ for both N_s^- and N_s^+ particles. (iv) At higher rapidities, $Y_{\text{lab}} > 6{\cdot}0$, R_{em} for N_s^+ particles in figure 10 (b) is $\geqslant 1$ while the N_s^- data show a clear depression with the magnitude being around $\sim 0{\cdot}4$. This shows a strong attenuation effect.

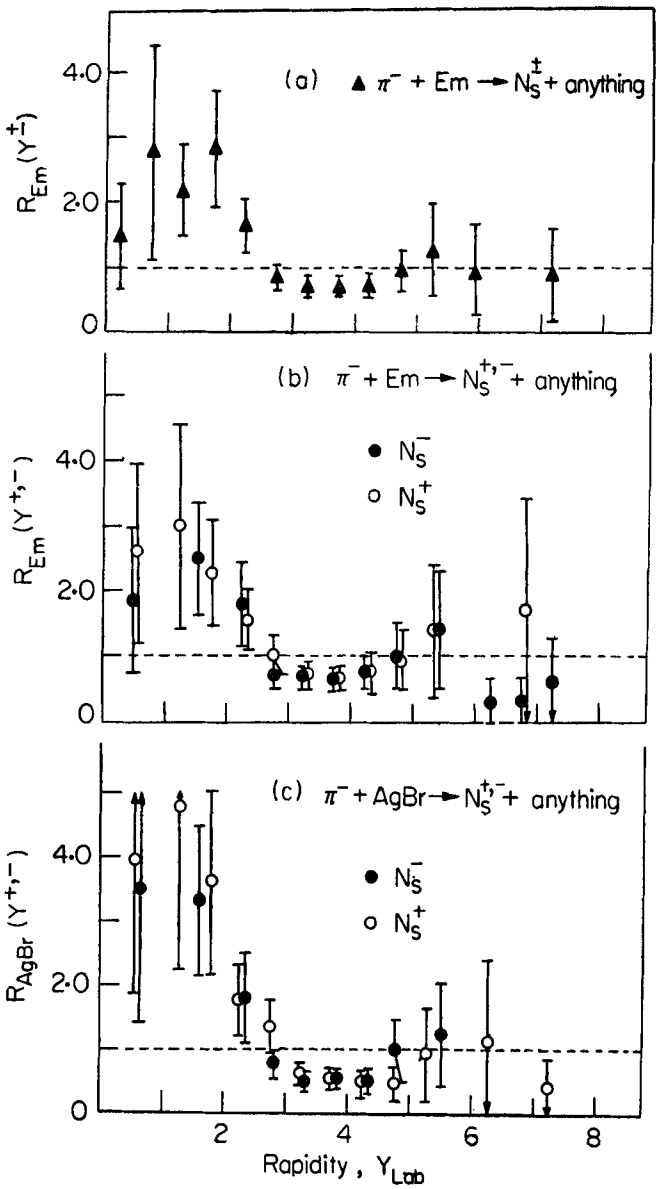

Figure 10. Normalised mean multiplicity R_{em} (Y_{lab} versus rapidity Y_{lab} plots for combined $N_s^{\pm}$ particles (b) R_{em} (Y_{lab}) plots for N_s^- and N_s^+ particles separately in case of π-Em collision and (c) R_{AgBr} (Y_{lab}) plots for N_s^- and N_s^+ particles in π^--AgBr events.

In figure 10 (c), the data in all Y_{lab} bins show similar trends as in figure 10 (b). In the target region $R_{(N_h \geq 8)} \equiv R_{(AgBr)} \simeq 3{\cdot}5$ at all $Y_{lab} \leqslant 2{\cdot}0$. In the central dip region $R_{AgBr} \simeq 0{\cdot}50 \pm 0{\cdot}20$ which is less than R_{em} in this Y-region. This may be attributed to the fact that the average AgBr nucleus is much larger than the average emulsion nucleus, and hence a larger absorption of created particles.

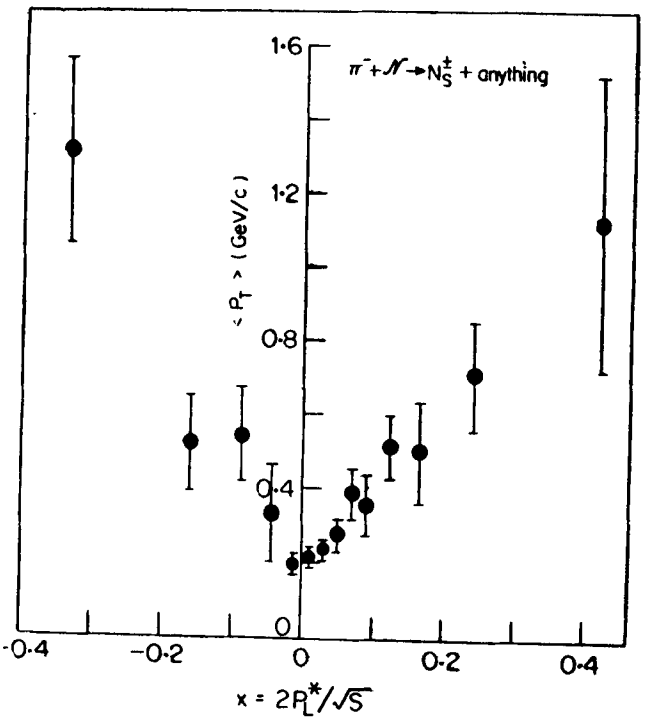

Figure 11. Seagull effect plot for combined $N_s^{\mp}$ multiplicity in π^- -nucleon like ($N_h \leqslant 1$) events.

3.3 *Seagull effect*

In figure 11, a characteristic correlation between the Feynman variable $X = 2P_L^*/\sqrt{s}$ and a Lorentz invariant $\langle P_T \rangle$ (P_L^* being the longitudinal momentum in CMS and $\sqrt{s}$ being the centre of mass energy) has been displayed for π^--nucleon reactions of our data. $\langle P_T \rangle$ has been evaluated over the whole phase-space. The characteristic feature of the distribution is that it shows a sharp reduction of $\langle P_T \rangle$ at $X = 0$ and as X increases in either direction there is a rapid increase in $\langle P_T \rangle$. Such a character of multiparticles is known as 'seagull effect'. From the figure it is clear that the large P_T particles fall towards large X-values. The effect has been noted even at smaller primary energies, say in 7·5 GeV π^--p collision by Balyskov and Kladnitskaya (1967), in 19·2 GeV p-nucleon collision by Takibaev *et al* (1976) and in 40 GeV/c π^--nucleon collision by Angelov *et al* (1977). The dip at $X = 0$ follows the conservation of momenta and reflects that the multiparticle production takes place through the formation of intermediate states.

4. Conclusions

From the present study of 50 GeV/c π^--collision with emulsion nuclei, the following conclusions may be drawn;

(i) The contribution of target mass in multiparticle production is significantly large which is contained mostly in the small momenta and rapidity regions. In support of it, the P_{lab}, P_L, P_T and Y_{lab} data in figures 3, 4, 6 and 8 and the average net charge data in figure 5 show an excess of positive charge in small P_{lab}, P_L, P_T and Y_{lab} regions. Thus the possibility that an excess positive charge may be due to the ejection of target protons may not be ruled out. Yeager *et al* (1977) in a 10·5 GeV/c π^--Ne^{20} experiment have detected a large proton production at small rapidities.

(ii) The invariant cross-section of both N_s^- and N_s^+ particles in the range $P_T \leqslant 0{\cdot}6$ GeV/c follows an exponential fall. It supports the thermodynamical statistical approach. The large P_T data (2·0 GeV/c) follows a $\sim P_T^{-4}$ power law, indicating the role of the constituent quarks of the colliding hadrons.

(iii) The leading N_s^- particle multiplicity is significantly depressed in π^--A collision as against the π^--nucleon collision. In π^--C^{12} collision at 40 GeV/c momentum it is observed by Aleiv *et al* (1978) that $R(Y) \simeq 0{\cdot}8$ for π^--particles in high momentum region (leading pions) while in our experiment this value is $\simeq$ 0 40 in 50 GeV/c π^--e m^{73} collision. It may, therefore, be inferred that leading pion is attenuated much more strongly in heavier nucleus. In a separate study of multiplicity-scaling by Kumar *et al* (1978) it has been observed that leading pion multiplicity is approximately zero in π^--A collision.

(iv) The observations (figure 10) that (a) a significant number of created particles are absorbed in the nuclear mass itself, (b) a plateau in $4{\cdot}75 < Y_{lab} \leqslant 6$ region and (c) attenuation of leading pion (π^-) in high rapidity region all depict a space-time development picture of the hadronic matter. Such a development seems to follow the additive quark model of multiparticle production off the heavy nuclei due to Nikolaev *et al* (1978).

Acknowledgements

The authors are grateful to Profs S Lyubomilov and K D Tolstov of JINR, Dubna (U.S.S.R) and to Dr J M Kohli of Panjab University, Chandigarh for their help in the exposure and despatch of the nuclear emulsion stack from U.S.S.R. They are also thankful to Profs P K Malhotra, A Subramanian and D S Narayan at TIFR, Bombay for useful discussions. VK thanks C S I R for a post-doctoral fellowship, N S V thanks U G C for a teacher fellowship, S C V and N S V also thank their respective college authorities.

References

Angelov N *et al* 1977 *Sov. J. Nucl. Phys.* **26** 294

Aliev F K, Inogamov Sh V, Yuldashev A A, Uldashev B S and Nikolaev N N 1978 Preprint TH-2511-CERN

Ammosov V V *et al* 1973 *Nucl. Phys.* **B58** 77

Berman S M, Bjorken J D and Kogut J B 1971 *Phys. Rev.* **D4** 3388

Balyskov V A and Klsdnitskaya E N 1967 *Sov. J. Nucl. Phys.* **5** 592

Chung Ta Meng 1977 *Phys. Rev.* **D15** 197
Danysz M, Garbowska K, Saniewska T and Skrzypezak E 1963 *Nucl. Instrum. Method.* **24** 103
Feynman R P 1969 *Phys. Rev. Lett.* **23** 1415
Gottfried K 1973 *Fifth Int. Conf. on High Energy Phys. and Nuclear Structure, Uppsala.*
Gunion J F, Brodsky S J and Blankenbecler R 1972 *Phys. Rev.* **D6** 2652
Kumar V, Sharma A P, Kaur M, Kohli J M, Mittra I S and Sood P M 1978 *J. Phys. Soç. Jpn.* **44** 1078
Kumar V, Varma S C, Verma N S and Sharma A P 1978 *Pramana* **11** 479
Kumar V 1979 *Study of multiparticle production in* 50 *GeV/c—interaction with emulsion nuclei*, Ph.D. Thesis, Kurukshetra University, Kurukshetra (submitted)
Nikolaev N N, Ostapehuk a Ya and Zollar V R 1978 Preprint TH-2541-CERN
Takibaev Zh S, Boo E G, Zhautykov B O, Mosienko A M and Tursunov R A 1976 *Sov. J. Nucl. Phys.* **24** 513
Tolstov K D and Shabratova G S 1974 Preprint R1-8402-JINR, Dubna
Vionov V F *et al* Alma-Ata, Dubna, Leningrad, Moscow and Tashkent Collaboration (1975 *JETP Lett.* 22 24)
Vinov V F *et al* 1977 *Sov. J. Nucl. Phys.* **27** 533; **26** 653
Yeager W M *et al* 1977 *Phys. Rev.* **G16** 1294